Journal of Applied Fluid Mechanics, Vol. 17, No. 5, pp. 1083-1098, 2024.
Available online at www.jafmonline.net, ISSN 1735-3572, EISSN 1735-3645.
https://doi.org/10.47176/jafm.17.05.2193

Sessile Droplet Evaporation on Wall with Radial Temperature Gradient

Z. G. Lei[1], C. Q. Shen[2], C. C. Song[2], F. Yao[3] and X. D. Liu[1,2†]

[1] *Zhejiang Juhua Technology Center Co., Ltd, Quzhou 324004, PR China*
[2] *College of Electrical, Energy and Power Engineering, Yangzhou University, Yangzhou 225127, PR China;*
[3] *Jiangsu Key Laboratory of Micro and Nano Heat Fluid Flow Technology and Energy Application, School of Environmental Science and Engineering, Suzhou University of Science and Technology, Suzhou, Jiangsu 215009, PR China*

†Corresponding Author Email: liuxd@yzu.edu.cn

ABSTRACT

Droplet evaporation coupled with gravity and surface tension on a wall with the radial temperature gradients is numerically studied with the arbitrary Lagrangian–Eulerian method. The influence of the wall temperature distribution on the droplet evaporation process, which is less considered in the existing literature, is mainly discussed. The droplet temperature coefficient of the surface tension and the viscosity on the droplet profile evolution, flow, heat and mass transfer characteristic are also discussed. The results indicate that the droplets become flat first and then retract under the gravity and Marangoni convection during droplet evaporation. There are two high-velocity regions inside the evaporating droplet. One region is at the droplet axis, in which fluid flows to the wall from the droplet top. The other region is near the droplet surface, where fluid flows to the droplet top. There are turning points on the two sides of which the influence of wall temperature distribution on the ratio between the droplet height and the radius of the three-phase contact line (h/R_c), the velocity in the droplet and the surface temperature converts. All of them are larger before the turning point when the wall temperature slope is positive. After the turning point, these are reversed. For both h/R_c and average surface temperature, there is one turning point, which are $t^*=1.63\times10^{-4}$ and $t^*=1.05\times10^{-4}$, respectively. For maximum velocity and average velocity in droplet, there are two turning points, which are both $t^*=1.63\times10^{-4}$ and $t^*=1.7\times10^{-5}$. The droplet morphology changes more obviously when it is with a greater temperature coefficient of surface tension. Moreover, the turning point is delayed from $t^*=6.41\times10^{-5}$ while α is 8 K/m to $t^*=7.91\times10^{-5}$ while α is -8 K/m, which indicates that the negative wall temperature slope is beneficial to inhibit the Marangoni effect on droplet evaporation.

Article History

Received August 2, 2023
Revised December 2, 2023
Accepted December 11, 2023
Available online February 24, 2024

Keywords:

Droplet evaporation
Radial temperature gradient
Marangoni convection
Arbitrary Lagrangian–Eulerian method
Simulation

1. INTRODUCTION

Droplet evaporation on walls is not only ubiquitous in nature but also a key thermophysical process in engineering applications, such as spray cooling (Zhang et al., 2013), thin-film preparation (Hu & Imaishi, 2000), ink-jet printing (Tekin et al., 2004), biomedical engineering (Hu & Larson, 2002), particle deposition and removal (Wang et al., 2001; Chang & Velev, 2006; Al-Sharafi et al., 2016a), and heat pump systems (Dai et al., 2019; 2023). During the evaporation process, an unbalanced surface tension distribution may be derived from the uneven surface temperature distribution on account of the nonuniform heat transfer led by the nonuniform droplet thickness and the inhomogeneous mass transfer on the surface. (Scriven & Sternling, 1960; Deegan et al., 1997) Then, Marangoni convection inside the droplets near the surface occurs. Simultaneously, the Marangoni convection reacts upon the distribution of droplet surface temperature distribution. Correspondingly, the mass transfer on the droplet is also impacted. Therefore, heat transfer, mass transfer and fluid flow are coupled during the evaporation process. A further study on the droplet evaporation flow, heat and mass transfer mechanism will not only contribute to improving the evaporation phase change theory but also provide an important theoretical basis and key technical support for droplet evaporation regulation in engineering

NOMENCLATURE

a	thermal diffusivity	T_{av}	droplet surface average temperature
c	mass concentration	T_c	wall temperature at the droplet center
C_p	the specific heat at constant pressure	T_{max}	maximum surface temperature
C_∞	boundary concentration of the gas phase	T_{min}	minimum surface temperature
D	diffusion coefficient	T_r	wall temperature at the three-phase contact line at the initial
f_{st}	force generated due to the interfacial tension	ΔT	difference between the average wall temperature and ambient temperature
F	external force	u	velocity vector
g	acceleration of gravity	u_g	gas velocity
h	maximum height of the evaporating droplet	u_l	liquid velocity
h^*	dimensionless droplet height	v_{av}	average velocity
H_v	latent heat of vaporization	v_{max}	maximum velocity
k	heat conductivity coefficient	**Greek symbols**	
k_g	thermal conductivity of the gas phase	α	wall temperature slope
k_l	thermal conductivity of the liquid phase	θ	contact angle
M_f	mass flux at the interface	μ	dynamic viscosity
M_a	Marangoni number	ν	kinematic viscosity
p	pressure	ρ	density
Q	heat of evaporation	ρ_g	gas density
r^*	dimensionless three-phase contact line radius	ρ_l	liquid density
R_c	radius of the three-phase contact line	σ	surface tension
R_{ci}	initial radius of the three-phase contact line	σ_r	surface tension at the three-phase contact line
t	time	σ_T	temperature coefficient of the surface tension
t^*	dimensionless time	τ_g	gas phase total stress tensors
T	temperature	τ_l	liquid phase total stress tensors
T_{abm}	ambient temperature		

practice. In this case, it can improve the performance of related devices to increase the utilization rate of materials and energy, which is very meaningful to achieve the goal of carbon neutrality.

To date, considerable attention has been given to droplet evaporation on heated walls. Deegan (2000b) and Deegan et al. (1997, 2000) indicated that since the thickness is larger at the center than at the droplet edge, the center surface temperature is lower than edge under a larger heat transfer resistance. Moreover, the hot fluid will flow to the droplet top from the edge driven by the unbalanced tension along the surface due to this uneven surface temperature distribution (Tsoumpas et al., 2015; Shi et al., 2017; Strizhak et al., 2018). Chandramohan et al. (2016), Albernaz et al. (2016) and Savino et al. (2002), and Savino & Fico (2004) found that the Marangoni convection coupled with the surface evaporation mass transfer and heat transfer during droplet evaporation and that the Marangoni convection dominates and strengthens the heat transfer and impairs the surface temperature nonuniformity. Simultaneously, the redistribution of the fluid induced by the Marangoni convection will cause fluctuation (Girard et al., 2006, 2008), deformation (Thiele & Knobloch, 2004) and other dynamic behaviors of the droplet surface. For example, the Marangoni vortex drives fluid aggregation from the droplet edge to the center (Xu et al., 1984; Quo et al., 1985; Guéna et al., 2007; Tsoumpas et al., 2015), which leads to differences from classical large droplets. The Marangoni convection also impacts the droplet size during evaporation. A simulation conducted by Barmi & Meinhart (2014) indicated that as the droplet volume and surface temperature gradient decrease, the Marangoni convection gradually weakens until it is negligible. In addition, the flow in the evaporation droplet is also impacted by the wall wettability. Droplet evaporation on wall with different contact angle is numerically investigated by Hu & Larson (2005, 2006) and found that there is a critical contact angle where the droplet surface temperature distribution flips. The surface temperature rises to the edge from top if the contact angle is over a critical value. On the contrary, the surface temperature distribution trend will reverse. Wang & Shi (2020) found that in the region of the three-phase contact line, the surface temperature gradient is greater under a larger contact angle. The gradient direction is also affected by the critical contact angle, which depends on both the ratio of the substrate thickness to the droplet contact line radius and the relative thermal conductivity of the substrate and the droplet (Ristenpart et al., 2007; Xu et al., 2012). Zhu et al. (2019) found that thermocapillary convection always takes place near the three-phase contact line as long as the temperature gradient exists, which stabilizes the occurrence of the Marangoni convective instability. Al-Sharafi et al. (2016b) found

that the Marangoni convection dominates the flow inside a droplet when it is on a substrate with high contact angles.

The wall temperature distribution is an important boundary condition for droplet evaporation. However, most researchers have focused on the influences of the physical property parameters and contact angles on droplet evaporation on walls with uniform temperature (Liu et al., 2023; Sefiane et al., 2008). At present, studies on the impact of the wall temperature distribution characteristics on droplet evaporation are still limited, and most of them are about uniform wall temperatures. Nevertheless, droplet evaporation often occurs on nonuniform temperature walls in real applications, such as spray cooling technology for nonuniform internal heat source electronic equipment (Zhang et al., 2009), surface cooling of metal processing (Kus et al., 2015) and cell deposition processes in PCR chip laboratories (Shi et al., 2011). Simultaneously, it is worth noting that nonuniform heat transfers inside droplets due to nonuniform temperature walls and droplet thicknesses will trigger the Marangoni convection inside droplets. Therefore, the wall temperature characteristics also have an important effect on the heat and mass transfer processes. It is necessary to investigate the influence mechanism and characteristics of the wall temperature distribution on the droplet evaporation. For instance, in an experiment Kita et al. (2016) obtained a nonuniform wall temperature distribution by laser heating the lower wall where the droplet evaporates and observed vortex oscillation in the droplet, which is not observed in droplet evaporation at a uniform wall temperature. However, the characteristics of the wall temperature distribution are difficult to describe quantitatively. Additionally, how the wall temperature distribution affects the droplet evaporation process still needs to be further understood. For this purpose, compared to the experimental study, numerical simulation is a good method to probe the mechanism of the evaporation process. Molecular dynamics simulation (Zhang et al., 2019; Huang et al., 2022) is an effective method. However, due to limitations in the computational power, the droplet size that is used in the simulation is always small. Therefore, in the current study, droplet evaporation on a wall with a radial temperature gradient is numerically investigated based on the arbitrary Lagrangian-Euler (ALE) formulation (Yang et al., 2014). The morphology and the temperature and velocity distributions, especially the Marangoni effect in droplets during the evaporation process, are presented. It is worth mentioning that a turning point in which the influence of the wall temperature distribution on the evaporation process changes is found.

2. PHYSICAL AND MATHEMATICAL MODELS

2.1 Assumptions

Some assumptions are considered as follows:

(1) Since the velocity is low, the flow is considered to be laminar and incompressible.

(2) In the current study, the Bond number (Cheng & Wu, 2006) is about 0.2. Thus, the gravity cannot be neglected.

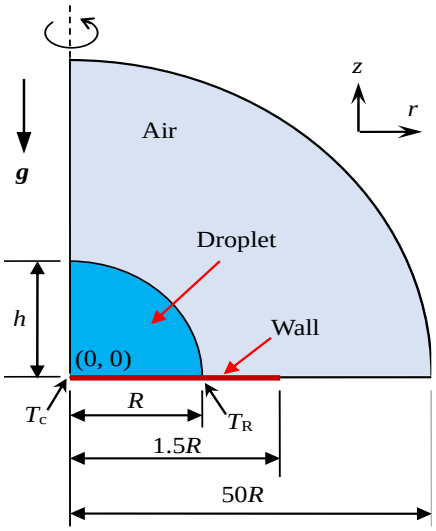

Fig. 1 Diagram of the computational domain

Table 1 Physical parameters of HFE7100 (Machrafi et al., 2018; Bi et al., 2016)

Physical parameters	value
Density (ρ)	1482 (kg/m^3)
Kinematic viscosity (v)	5.914e-7 (m^2/s)
Constant pressure specific heat capacity (C_p)	1183 (J/kgK)
Surface tension coefficient at 293K (σ).	0.0393 (N/m)
Latent heat of vaporization (H_v)	1.116e5 (J/kg)
Diffusion coefficient at 298K (D).	6.98e-6 (m^2/s)

(3) Except the temperature coefficient of the surface tension (σ_T), physical parameters are set to be constant.

2.2 Physical Model

Considering the Marangoni effect, the ALE formulation method is used to establish a model to trace the droplet evaporation process on a surface with a radial temperature gradient. As shown in Fig. 1, an axisymmetric quarter circle region of 50R is adopted as the computational domain. The sessile HFE 7100 droplet is on the horizontal wall whose radius is 1.5R. The physical parameters of HFE 7100 are listed in Table 1.

2.3 Governing Equations

The governing equations involved in the model for droplet evaporation used in the current study are as follows:

The incompressible N–S equation in fluid is as follow (Yang et al., 2014):

$$\rho\left(\frac{\partial \boldsymbol{u}}{\partial t}+\left(\boldsymbol{u}_c\cdot\nabla\right)\boldsymbol{u}\right)=\nabla\cdot\left[-p\boldsymbol{I}+\mu\left(\nabla\boldsymbol{u}+\left(\nabla\boldsymbol{u}\right)^T\right)\right]+\boldsymbol{F}+\rho\boldsymbol{g} \quad (1)$$

where ρ, $\mathbf{u}$, t, p and μ are the density, velocity, time, pressure and dynamic viscosity, respectively.

The continuity equation is (Yang et al., 2014):

$$\nabla \cdot \boldsymbol{u} = 0 \tag{2}$$

The diffusion equation in gas is (Yang et al., 2014):

$$\frac{\partial c}{\partial t} + (\boldsymbol{u}_c \cdot \nabla)c = \nabla \cdot (D\nabla c) \tag{3}$$

in which c represents the molar concentration.

In the whole computation domain, the heat transfer equation is as follows (Yang et al., 2014)

$$\rho C_p\left(\frac{\partial T}{\partial t} + (u_c \cdot \nabla)T\right) = \nabla \cdot (k\nabla T) \tag{4}$$

in which k and T are the thermal conductivity and temperature, respectively.

2.4 Initial Conditions and Boundary Conditions

2.3.1 The initial conditions

The initial velocity in fluid is set as

$$u_0 = 0 \tag{5}$$

The ambient pressure and temperature are set to be initial pressure and temperature:

$$T_0 = T_{amb} \tag{6}$$

$$p_0 = p_{amb} \tag{7}$$

T_{amb} and p_{amb} are 293 K and 101325 Pa, respectively.

The initial concentration in the gas phase is as follows:

$$c_0 = 0 \tag{8}$$

In addition, there is no grid displacement in the initial stage.

Droplet evaporation on the wall is coupled with heat transfer, fluid flow and mass transfer, which involves the movement of the three-phase contact line and gas–liquid interface. The boundary conditions are described as follows.

2.3.2 The boundary conditions of laminar two-phase flow

The Axisymmetric is set at r=0: (Yang et al., 2014)

$$\boldsymbol{u} \cdot \boldsymbol{n} = 0 \tag{9}$$

$$\left[-P\boldsymbol{I} + \mu\left(\nabla \boldsymbol{u} + (\nabla \boldsymbol{u})^T\right)\right] \cdot \boldsymbol{n} = 0 \tag{10}$$

On two-phase interface, the stresses are balanced as follows (Yang et al., 2014):

$$\boldsymbol{n} \cdot \boldsymbol{\tau}_g = \boldsymbol{n} \cdot \boldsymbol{\tau}_l + \boldsymbol{f}_{st} \tag{11}$$

In the tangential direction of the interface, the following can be obtained (Yang et al., 2014):

$$\left(\boldsymbol{n} \cdot \boldsymbol{\tau}_g - \boldsymbol{n} \cdot \boldsymbol{\tau}_l\right) \cdot \boldsymbol{t} = -\sigma_T \nabla_s T \tag{12}$$

in which τ is the stress tensor and σ is the surface tension.

The relationship between the flow velocity and the mass flow at the droplet surface is as follows (Scardovelli, & Zaleski, 1999):

$$\boldsymbol{u}_1 = \boldsymbol{u}_2 + M_f\left(\frac{1}{\rho_g} - \frac{1}{\rho_l}\right)\boldsymbol{n} \tag{13}$$

In the above equations, $\boldsymbol{\tau}_g$ and $\boldsymbol{\tau}_l$ are the gas liquid phase total stress tensors. $\boldsymbol{f}_{st}$ is the force generated due to the interfacial tension. $\boldsymbol{t}$ is the tangential vector. $\boldsymbol{u}_g$ and ρ_g are the gas velocity and density, respectively, and $\boldsymbol{u}_l$ and ρ_l are the liquid velocity and density, respectively. M_f is the mass flux.

In the current study, vapor at the droplet surface is treated as saturated, and the vapor saturation pressure of HFE 7100 is calculated as follows (Manetti et al., 2020):

$$\ln P = 22.415 - 3641.9\frac{1}{T} \tag{14}$$

The Navier slip boundary condition (Xu et al., 2018) is used for the wall, and the length of the slip packet is 2 μm. The pressure at the edge of the gas phase area is set to 1 atm.

2.3.3 The heat transfer boundary conditions

At r=0, axisymmetric conditions are applied as follows (Yang et al., 2014):

$$-\boldsymbol{n}\ (-k\nabla T) = 0 \tag{15}$$

Since evaporation occurs, the latent heat across the interface should be considered, where the boundary condition is as follows (Yang et al., 2014):

$$\boldsymbol{n} \cdot \left(k_g(\nabla T)_g - k_l(\nabla T)_l\right) = Q \tag{16}$$

in which k_g and k_l are the gas thermal conductivity and liquid thermal conductivity. Q is the heat of evaporation, and $Q = -M_f H_v$, where M_f and H_v are the total evaporation rate and latent heat, respectively.

The wall is set as the temperature boundary condition, and the temperature distributions are evaluated according to this condition. The gas phase area edge temperature is

$$T_\infty = T_{amb} \tag{17}$$

2.3.4 The Mass Transfer Boundary Conditions

Axisymmetric conditions and non-flux boundary conditions are adopted at r=0 and the wall, respectively. Both are described as follows (Yang et al., 2014):

$$-\boldsymbol{n} \cdot (D\nabla c) = 0 \tag{18}$$

The outer boundary of the gas phase is the constant concentration boundary:

$$c_\infty = 0 \tag{19}$$

2.5 Grid Independence Test

To adapt to the boundary conditions well, the calculation area is divided by the unstructured triangular mesh. Additionally, the mesh at the droplet surface and

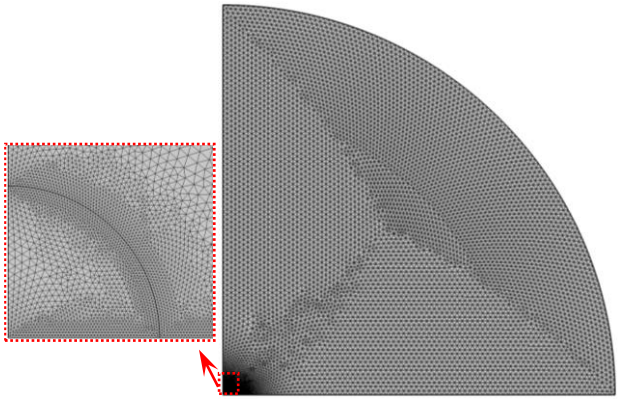

Fig. 2 Mesh for droplet with radius of 0.75 mm

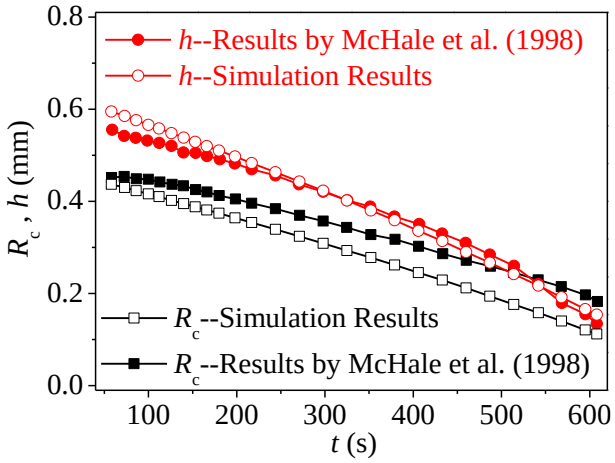

Fig. 3 Comparison of the maximum height and contact radius of evaporating droplets between simulations in the current study and experiments by McHale et al. (1998).

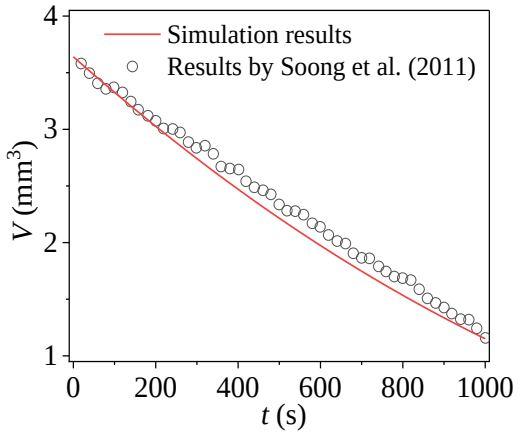

Fig. 4 Comparison of the droplet volume between simulations in the current study and experiments by Song et al. (2011)

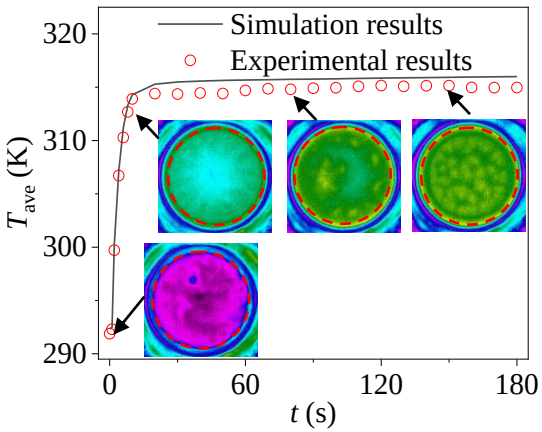

Fig. 5 Comparison of the average surface temperature of evaporating film between simulation results and infrared visualization results

wall are refined. For example, when the droplet radius is 0.75 mm, after the grid independence test, the total number of selected grids is 21150, including 2673 droplet areas, as shown in Fig. 2.

2.6 Model Validation

In order to validate the model used in the current study, the experiment and numerical studies of water droplet evaporation are compared. Figure 3 shows the comparison of profile of droplet with the initial droplet radius of 0.488 mm and the contact angle of approximately 108° during the evaporation process (McHale et al., 1998). The average errors of the contact radius and maximum height between simulation in the current study and in experiment are 16.2% and 4.9%, respectively. As shown in Fig. 4, it compares the volume evolution of evaporation water droplet on wall with the contact angle of 57° in still air during the experiment conducted by Song et al. (2011) and the simulation based on the model in the current study. It is found that the average errors of the droplet volume between simulation and in experiment is about 4.8%. In addition to the droplet evaporation, the comparison of average surface temperature of HFE 7100 film between the experimental results and the simulation results based on the model in the current study is also proposed, as shown in Fig. 5. The film with the thickness of 1.5 mm is in a cavity with the diameter of 20mm, and the cavity is heated at the bottom where the temperature is adjusted to 318 K. It can be seen that the simulation results and the infrared visualization results are very closed.

Furthermore, under constant contact angle mode, Erbil et al. (2002) carried out a theoretical analysis on the evolution of droplet volume, which is influenced by the surface contact angle, droplet physical properties and concentration in the environment. Figure 6 shows a comparison of the numerical simulation and theoretical model results. It is indicated that under droplet contact angles of 30°, 60°, 90° and 120°, the average errors between the results by model and simulation results are 8.9%, 4.9%, 7.3%, and 10.9%, respectively.

By comparing the numerical simulation results with those in literatures, it can be considered that the model adopted in the current study is reliable. In addition, a droplet contact angle of 90° is adopted in the current study.

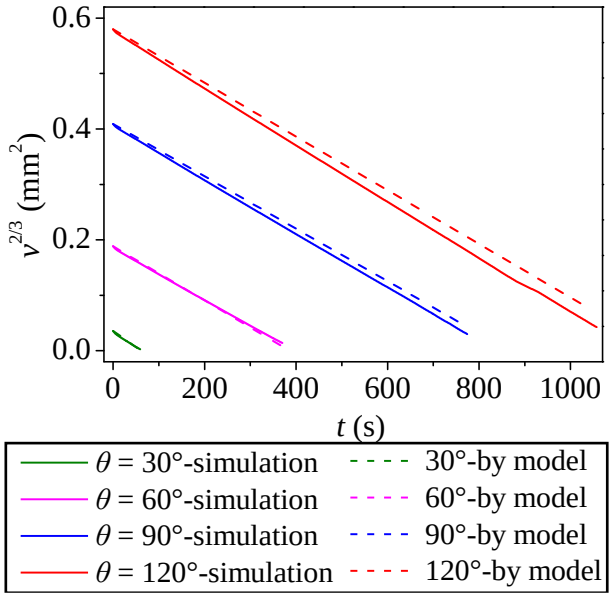

Fig. 6 Comparison of the volume change of evaporating droplets between the simulation in the current study and the model by Erbil et al. (2002)

3. RESULTS AND DISCUSSION

To quantify the droplet evaporation process, dimensionless time, dimensionless three-phase contact line radius, and dimensionless droplet height are used as follows (Gao et al., 2018):

$$t^*=Dt/R \tag{20}$$

$$r^*=R_c/R \tag{21}$$

$$h^*=h/R \tag{22}$$

In the equations above, t, D, R, and h are the time duration from the evaporation beginning, diffusion coefficient, droplet radius and height, respectively. The Marangoni number is also used in this study and is calculated as (Zhu & Shi., 2023)

$$Ma = \frac{\sigma_T \Delta T R_t}{\rho v a} \tag{23}$$

in which, R_t, ΔT, ρ, v and a are droplet radius, difference between the average wall temperature and ambient temperature, droplet density, droplet kinematic viscosity and droplet thermal diffusivity, respectively.

The wall temperature slope is defined as

$$\alpha = (T_r\text{-}T_c)/R_{ci} \tag{24}$$

T_c and T_r are the initial wall temperatures at the droplet center and edge, respectively, and R_{ci} is the initial three-phase contact line radius.

In addition, during the data analysis, significant digits are taken to one or two decimal places based on rounding. Therefore, there are errors in the results in this manuscript. Based on the data error analysis, the uncertainties of temperature, velocity in droplet, Maragoni number and h/R_c are about 0.3%, 2.5%, 0.73% and 0.95%, respectively.

3.1 Flow and Heat Transfer Characteristics During Droplet Evaporation on a Gradient Temperature Wall

Figure 7 shows the droplet profile during droplet evaporation on the wall with a contact angle of 90° and different wall temperature distributions. The mean wall temperatures of five cases are all 313 K. However, the wall temperature distribution is different. In Figs. 7(a) and (b), α is positive. The wall temperature distribution is uniform, and α is 0 in Fig. 7(c). In Figs. 7(d) and 7(e), α is negative.

The droplet evaporation processes on walls with different temperature distributions are similar. As evaporation progresses, the droplet volume gradually decreases. However, the evolution of droplet morphology is different during the evaporation process. For instance, by comparing the droplet profile at $t^*=1.09\times10^{-4}$, it can be seen that the droplet is the smallest when it evaporates on the surface with an α of 8 K/mm, as shown in Fig. 7(a). In contrast, when α is -8 K/mm, the droplets have the largest h and R_c, as shown in Fig. 7(e).

Correspondingly, Fig. 6 shows a comparison of the evolution of h/R_c on the surface with different α to represent the influence of the wall temperature distribution on the evaporation. The evolution of h/R_c involves three stages. Initially, under the impact of gravity, the droplet tends to flatten, and h/R_c rapidly decreases. In the next stage, the droplet begins to contract back as h/R_c rapidly decreases.

In the next stage, the droplet begins to contract back with increasing h/R_c. This is mainly due to two reasons. First, the droplet center thickness is greater than that of the edge. Hence, during the transfer of the teat to the droplet surface from the wall, the heat transfer resistance at the center is greater than that at the edge. For this reason, the droplet surface temperature monotonically increases to the top. This uniform surface temperature distribution will induce an unbalanced surface tension on the droplet surface, and drives the liquid to the droplet top. That is, the droplet height is intensified under the so-called Marangoni effect. In addition, the influence of gravity on the droplet morphology becomes weaker when the droplet size decreases. From Fig. 8, it is also indicated that h/R_c continues to increase when it is larger than 1. This indicates that droplet evaporation is markedly affected by the Marangoni effect. After h/R_c reaches its maximum, it is the third stage. In this stage, the droplet volume decreases. The decreasing droplet surface temperature gradient weakens the impact of the Marangoni effect on the droplet morphology. When the droplet becomes small enough, the effect of gravity is also attenuated. Therefore, h/R_c tends to decrease to 1. In addition, before $t^*=1.63\times10^{-4}$, h/R_c is larger for droplets on walls with a positive slope k of the wall temperature than for droplets on walls with a negative temperature slope. Moreover, h/R_c increases with increasing k. However, after $t^*=1.63\times10^{-4}$, the trend of h/R_c is reversed. In addition, the droplet morphology changes more

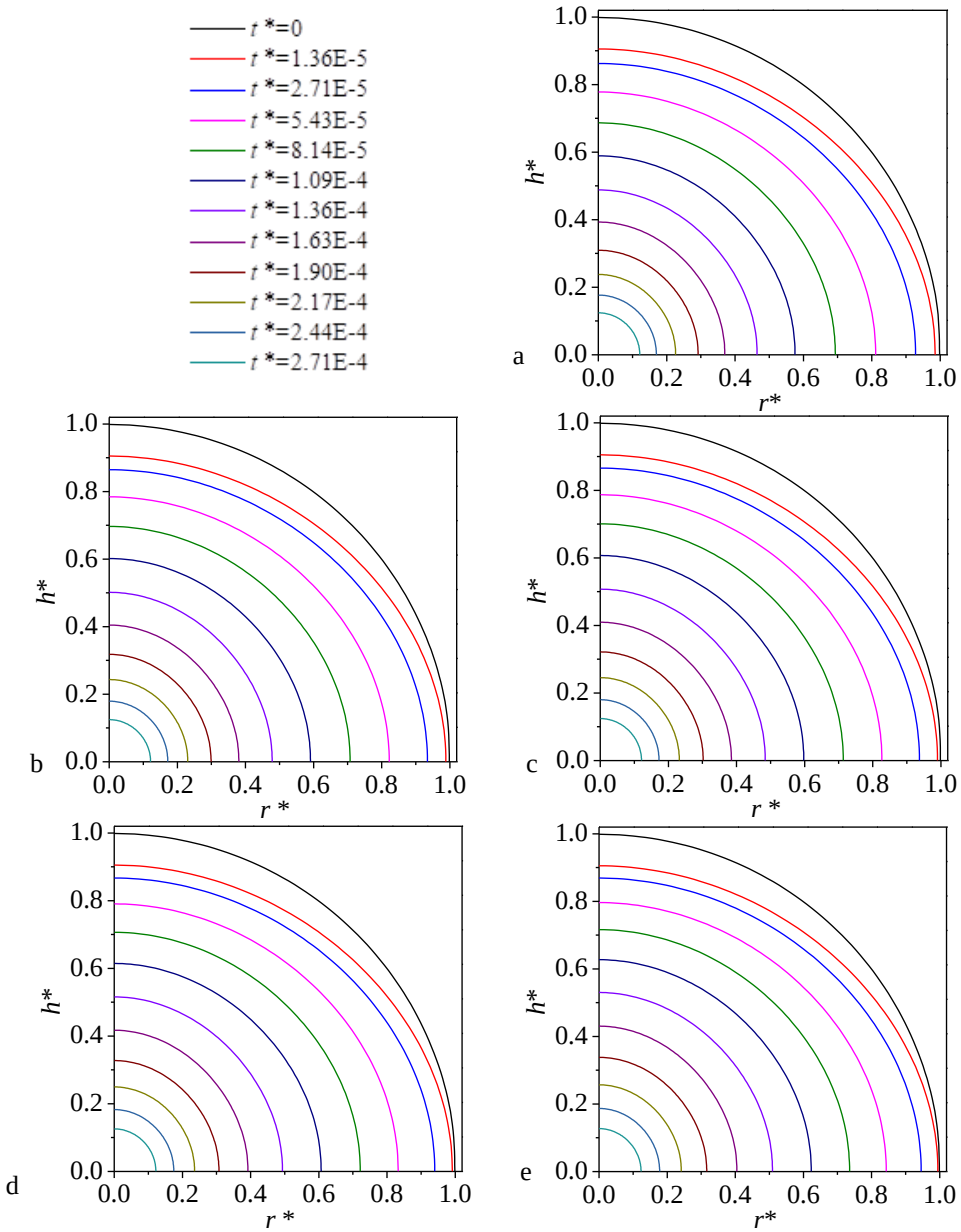

Fig. 7 Droplet profile evolution under different wall temperature distributions. (a) T_c=310 K, T_r=316 K, (b) T_c =312 K, T_r =314 K, (c) T_c =313 K, T_r =313 K, (d) T_c =314 K, T_r =312 K, (e) T_c =316 K, T_r =310 K

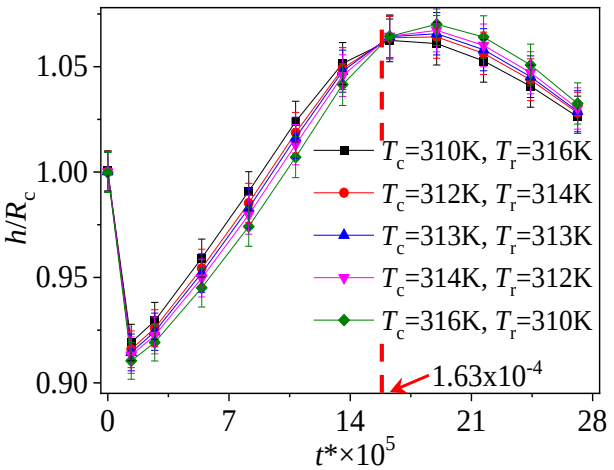

Fig. 8 h/R_c during the evaporation process for droplets on walls with different temperature distributions

Obviously when it is on a wall with a negative temperature slope. The minimum and maximum h/R_c is are 0.91 and 1.07 for droplet on wall with temperature slope of -8 K/mm. However, these are 0.92 and 1.06 for droplet on wall with temperature slope of 8 K/mm.

As mentioned above, the droplet morphology is affected by internal flow, which is strongly coupled with the temperature distribution. Figure 9 shows the internal flow and temperature distribution in droplet. The gradient surface temperature is induced by the nonuniform heat transfer cross droplet due to the nonuniform thickness. Thus, the Marangoni flow is generated by the gradient surface tension. Then, a counterclockwise vortex occurs in the droplet, which is consistent with the flow characteristic in sessile droplets when the Marangoni effect is considered (Yang et al., 2014). In the early stage, the vortex is located in the low-temperature region. The droplet inner temperature becomes uniform under the mixing of fluid.

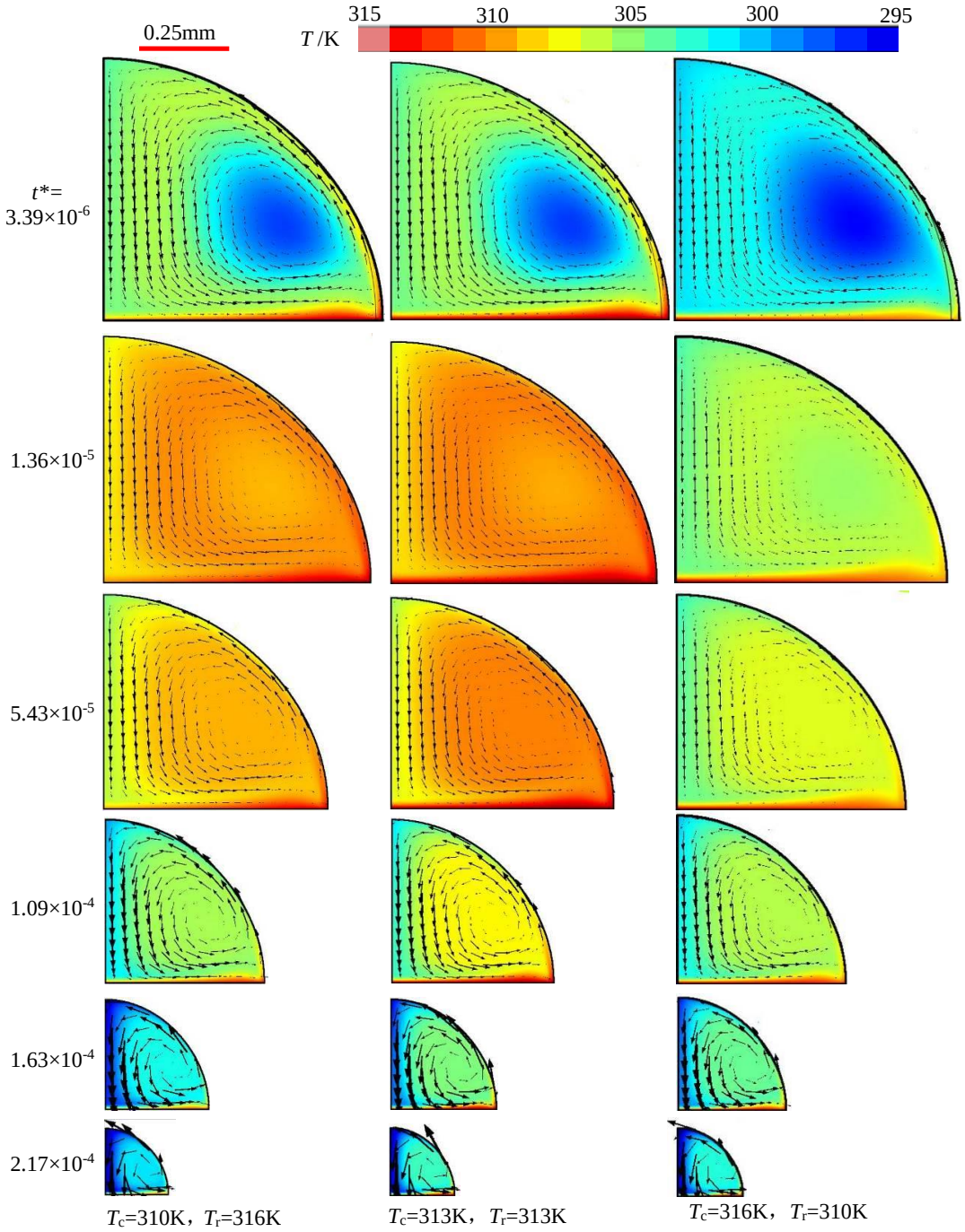

Fig. 9 Internal flow and temperature distribution in droplet

From Fig. 9, it is also found that the low and high temperature fluid flows downward along axis and to the top along the surface, respectively. Therefore, the low temperature region is at the center. As the droplet becomes small, the influence of evaporation on the droplet temperature reduction becomes increasingly obvious, and the overall droplet temperature gradually decreases. Furthermore, the surface temperature distribution is monotonic, while the top has the lowest temperature.

Heat transfer and flow are coupled when droplet evaporation occurs. Therefore, the wall temperature will affect the flow and inner droplet temperature. Figure 10 shows a plot of the average flow velocity and the maximum flow velocity in the droplet. It is shown that both rapidly increase when driven by gravity in a short time when the droplet starts to evaporate. However, with nonuniform heat transfer, a temperature gradient forms along the droplet surface and results in a corresponding unbalanced surface tension. Then, the Marangoni effect begins to counteract gravity, and the flow in the droplet weakens. However, above approximately $t^*=1.7\times10^{-5}$, when the Marangoni effect surpasses gravity, the average and maximum velocities will increase. When the volume of the droplet diminishes to a small enough value, the flow in the droplet decreases due to the increasingly obvious impact of viscous dissipation. In addition, similar to the evolution of h/R_c, before $t^*=1.63\times10^{-4}$, the average velocity (v_{av}) and maximum velocity(v_{max}) in the droplet are larger for the droplet on the wall with a positive slope k of the wall temperature than for the

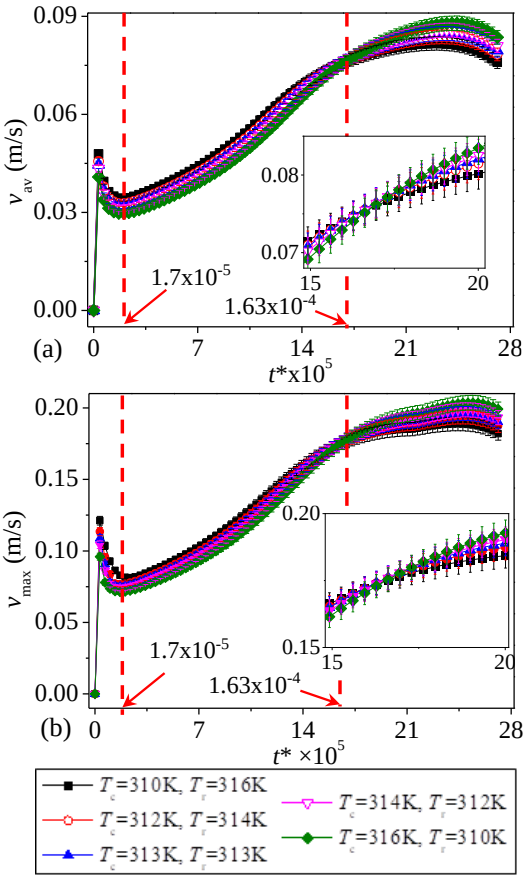

Fig. 10 Evolution of v_{av} and v_{max} in droplets during evaporation. (a) Average velocity. (b) Maximum velocity

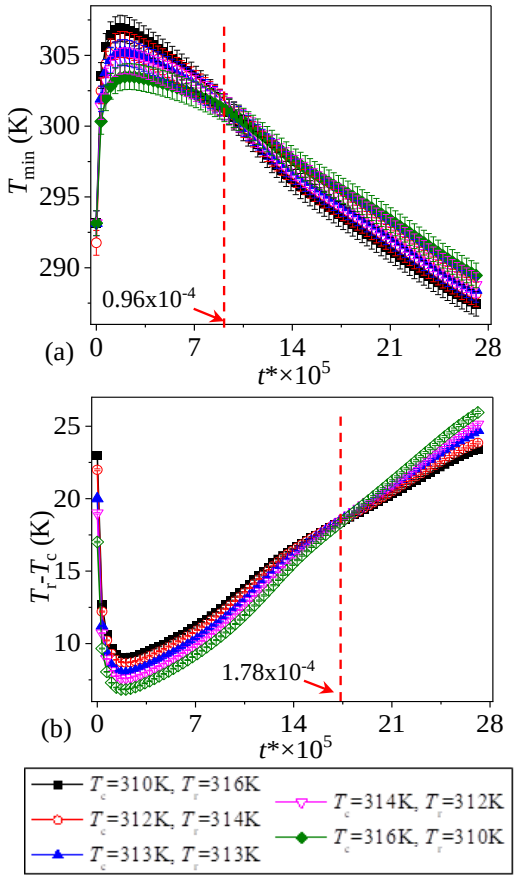

Fig. 11 Droplet surface temperature during evaporation on the wall with different temperature distributions. (a) Minimum surface temperature (T_{min}) and (b) T_r-T_t

droplet on the wall with a negative temperature slope. The velocity is larger for droplets on walls with higher α. Furthermore, after t*=1.63×10^{-4}, the trends of the average, maximum velocities, and h/R_c are reversed.

The Marangoni flow is induced and strongly impacted by surface temperature distribution. Figure 11 illustrates the minimum surface temperature (T_{min}) and the temperature difference between the three-phase contact line and droplet top (T_r-T_t). As seen from Fig. 11 (a), T_{min} rises to a peak value and then decreases. This is because the T_{min} is always within the droplet top. When heat is transferred through the droplet to the top and hot fluid flows to the top, the droplet top temperature gradually increases. However, the latent heat has an increasingly obvious influence on the droplet surface temperature during vaporization, especially when the droplet volume decreases. For this reason, T_{min} drops. During droplet evaporation, under the Marangoni effect, the fluid will flow to the droplet top. Thus, T_r-T_t has an important effect on this process. In Fig. 11 (b), T_r-T_t rapidly decreases from the beginning and soon increases during the evaporation process.

Figure 12 shows the evolution of the surface average temperature (T_{av}), which has the same characteristics as the minimum surface temperature. T_{av} rapidly increases due to heat transfer from wall after evaporation begins.

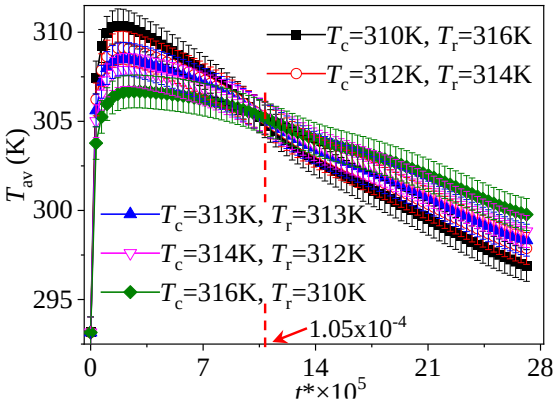

Fig. 12 Variation in the average surface temperature during droplet evaporation on the wall with different temperature distributions

Then, it decreases gradually. This is because evaporation occurs on the surface. Therefore, in addition to the wall temperature distribution, the surface temperature is greatly impacted by latent heat. Considering the thickness of the droplet, when heat transfers to the surface, the smallest resistance is at the droplet edge. Therefore, under the average wall temperature of 313 K and α>0, the high wall temperature region is at the edge, and heat transfer to the surface from

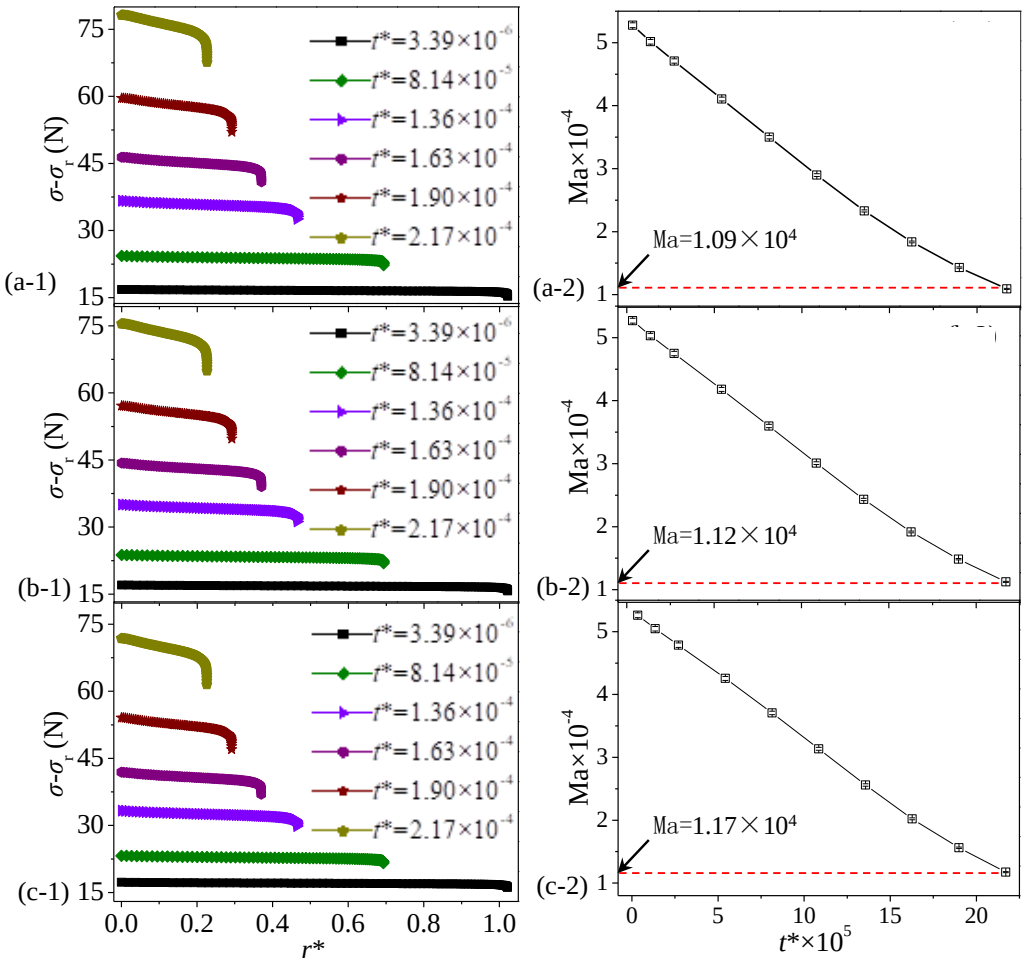

Fig. 13 Distribution of σ-σ_r and the evolution of Ma during the evaporation process. (a) T_c=310 K, T_r=316 K, (b) T_c =313 K, T_r =313 K, and (c) T_c =316 K, T_r =310 K

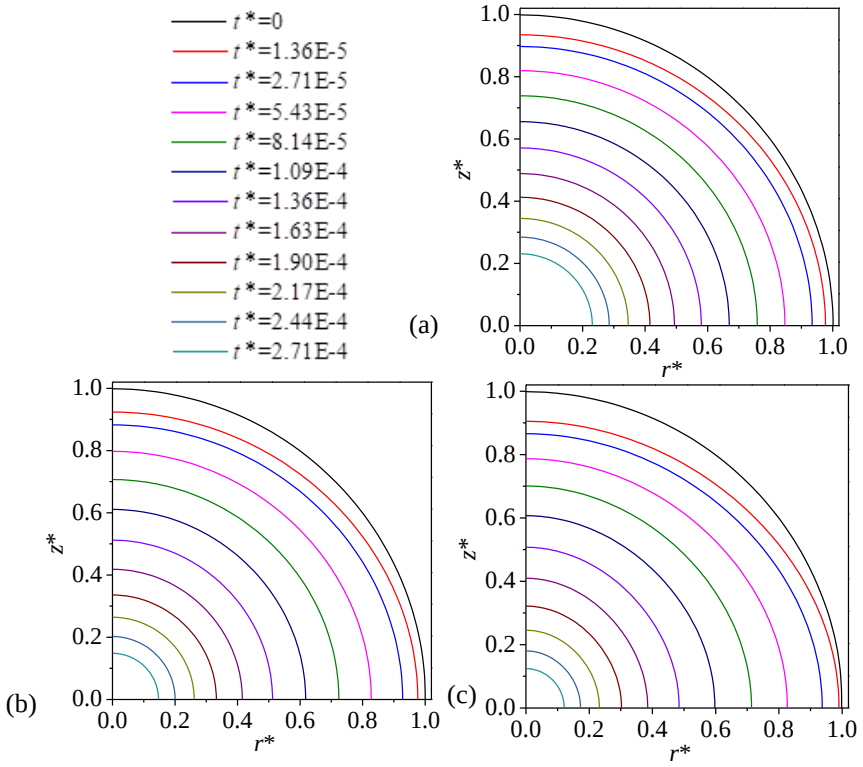

Fig. 14 Profile of the droplets with different temperature coefficients of the surface tension during the evaporation process. (a) σ_T = -8.5×10^{-6} N/mK, (b) σ_T = -4.85×10^{-5} N/mK, and (c) σ_T = -8.85×10^{-5} N/mK

the hot wall is more unhindered at the early evaporation stage. For this reason, T_{av} is higher when α>0. In contrast, at the later evaporation stage, the droplet becomes small enough due to evaporation mass transfer. Hence, the high wall temperature region is near the three-phase contact line when α<0. T_{av} is higher when α<0 at this stage. Furthermore, a closer observation of Figs. 11 and 12 indicates that there are turning points for the evolution of the evolution of T_{min}, T_{av} and T_r-T_t. The turning points are at approximately t^*=0.96×10^{-4}, t^*=1.78×10^{-4} and t^*=1.05×10^{-4}. Before the turning point, the surface temperature is higher for the droplet on the wall with a positive slope k than for the droplet on the wall with a negative temperature slope, and after the turning point, it is reversed.

By looking into the droplet surface tension distribution, it is found that the surface tension difference between the droplet surface and the three-phase contact line (σ-σ_r) decreases from the droplet top. In addition, σ-σ_r is greater when the droplet is on the wall with a positive temperature slope. Furthermore, σ-σ_r is enhanced s. However, due to the contraction of the droplet, Ma decreases during evaporation (Figs. 13 (a-2), (b-2) and (c-2)). That is, the Marangoni effect gradually weakens. The trends of σ-σ_r and Ma contribute to the evolution of the flow velocity in the droplet, as shown in Fig. 8.

3.2 Effect of the Temperature Coefficient of the Surface Tension

Since evaporation process is significantly impacted by the Marangoni flow, the Marangoni effect is investigated by changing the σ_T of the droplet, which are -8.5×10^{-6} N/mK, -4.85×10^{-5} N/mK and -8.85×10^{-5} N/mK in the current study. Figure 14 shows the droplet profiles with different σ_T values during the evaporation process. Droplet evaporation processes under different conditions are similar. However, the evaporation rate of droplets with a larger σ_T is higher, i.e., by comparing the profile at t^*=2.71×10^{-4} in Fig. 14. The r^* is 0.121 for droplets with σ_T of -8.85×10^{-5} N/mK, which is smaller than 0.231 for droplets with σ_T of -8.5×10^{-6} N/mK.

Figure 15 shows the h/R_c ratio for droplets with different σ_T, of which the evolution trend is the same as that mentioned above. However, for droplets with different σ_T, the droplet morphology during evaporation is still distinct. When σ_T is larger, the influence of the Marangoni effect is more pronounced. Thus, h/R_c is greater for droplets with larger σ_T in the later evaporation process. That is, the droplet is higher under the stronger Marangoni effect, which is similar to what Tsoumpas et al. (2015) found. Since heat and mass transfer are strongly coupled in evaporation, h/R_c is different for droplets on walls with different temperature distributions.

By comparison, it is found that the turning point is smaller when the droplet is on the wall with a positive temperature slope. As shown in Fig. 13, the turning point is t^*=6.41×10^{-5} for droplets on the wall with a positive temperature slope of α=8 K/mm (T_c=310 K, T_r=316 K), which is smaller than that (t^*=7.91×10^{-5}) for droplets on the wall with a negative temperature slope of α=-8 K/mm (T_c =316 K, T_r =310 K). This is because when α<0, the

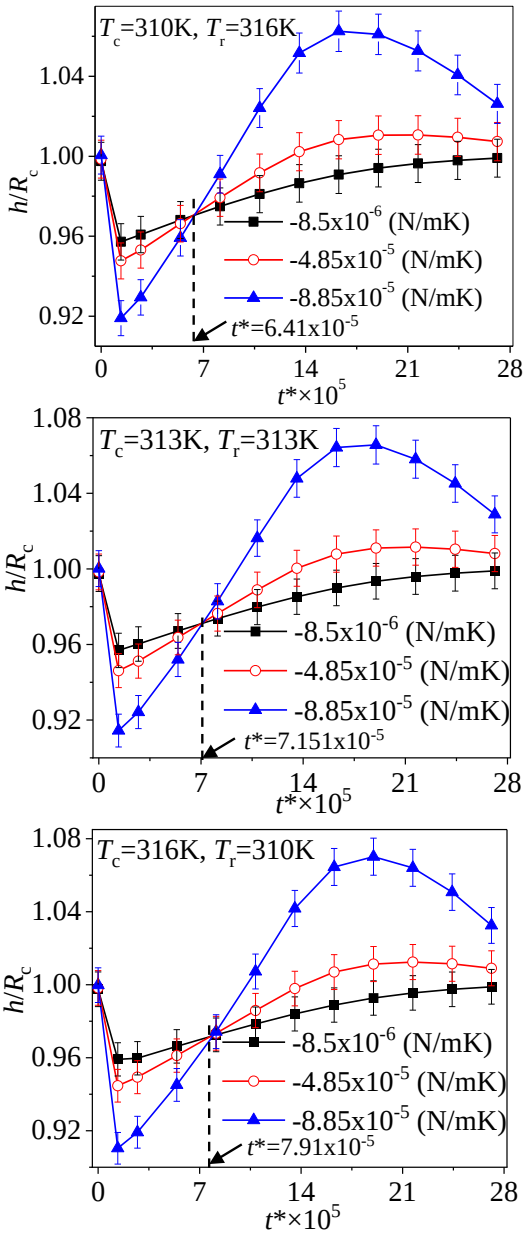

Fig. 15 h/R_c for droplets with different σ_T

droplet temperature at the edge is lower than that at the edge if the when α>0. In this case, the larger surface temperature gradient results in a higher surface tension gradient. Under a greater unbalanced force, the fluid is driven faster to the top from the droplet edge. This also indicates that the negative wall temperature slope is beneficial for inhibiting the Marangoni effect in droplets. That is, the wall temperature distribution is important for regulating the flow in evaporating droplets. This is very meaningful for droplet evaporation-related applications. For instance, the self-assembly of particles in droplets is significantly affected by the Marangoni flow (Bi et al., 2012; Nerger et al. 2020; Yin et al., 2023). Therefore, by adjusting the wall temperature distribution, the flow characteristics inside the droplet are regulated, and then different droplet deposition patterns are obtained.

Figure 16 shows a comparison of the flow inside droplets with different temperature coefficients of the surface tension. As mentioned above, the counterclockwise

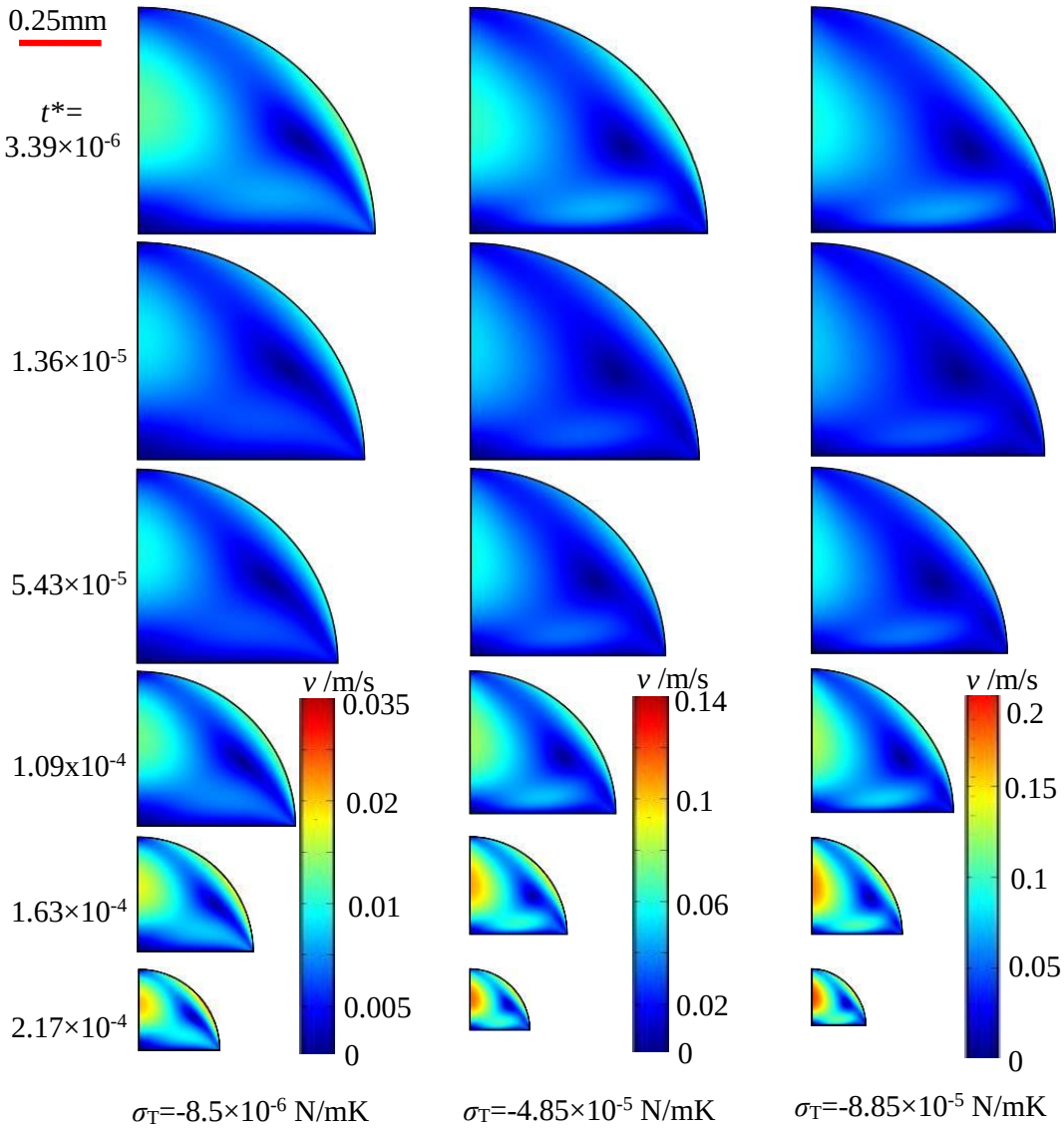

Fig. 16 Velocity distribution in droplets with different σ_T. (T_c=316 K, T_r=310 K)

Marangoni convective vortex always exists due to the gradient surface temperature. There are two high-velocity regions inside the evaporating droplet. One region is at the droplet axis, in which fluid flows to the wall from the droplet top. The other region is near the droplet surface, where fluid flows to the droplet top. As evaporation progresses, the flow velocity inside the droplet gradually increases. Furthermore, during evaporation, the Marangoni effect becomes stronger with increasing σ_T, and the internal velocity increases. Enhancement in internal flow is beneficial to evaporation mass transfer.

3.3 Effect of the Viscosity

Figure 17 shows the morphology evolution of droplets with different viscosities. Consistent with the above description, h/R_c in droplet evaporation experienced a process of first decreasing, then increasing, and then decreasing at different viscosities. However, for a droplet with a larger viscosity, the wall adhesion on the droplet is stronger to prevent the droplet from spreading on the wall under gravity. Therefore, h/R_c is larger. Figure 18 also indicates that the greater the viscosity of the droplet is, the more obvious the influence of viscosity resistance in the droplet, and the smaller the average and maximum velocity in the droplet during evaporation.

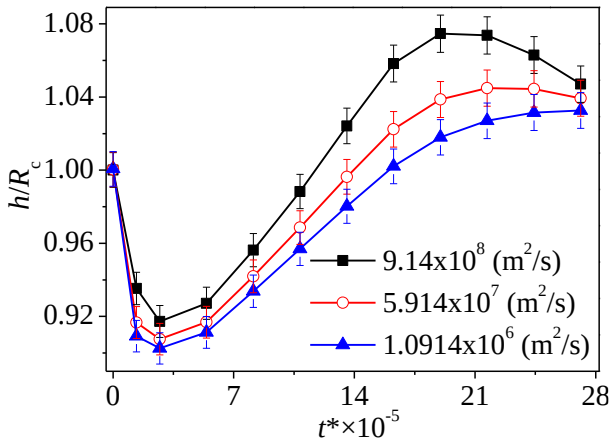

Fig. 17 h/R_c during the evaporation process for droplets with different viscosities

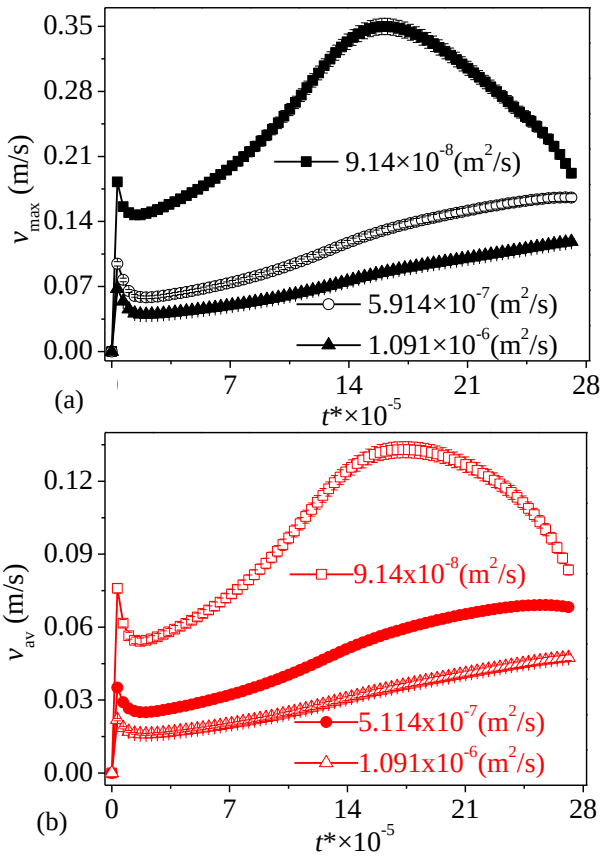

Fig. 18 Maximum and average velocity inside droplets with different viscosities. (a) maximum velocity, (b) average velocity

4. CONCLUSIONS

In order to explore how the wall temperature distribution affects the droplet evaporation process, a numerical study is conducted on the sessile droplet evaporation on a wall with radial gradient temperature by the arbitrary-Lagrangian–Eulerian (ALE) formulation method. The influence of the wall temperature distribution on the droplet evaporation process, which is less considered in the existing literature, is mainly discussed. The droplet temperature coefficient of the surface tension and the viscosity on the droplet profile evolution, flow, heat and mass transfer characteristic are also discussed. It is found that the negative wall temperature slope, when the wall center temperature is higher, is beneficial for inhibiting the Marangoni effect. The four main conclusions are as follows.

(1). Affected by gravity and Marangoni convection, the droplets become flat first and then retract during the evaporation process. The droplet morphology changes more obviously when it is on a wall with a negative temperature slope. The minimum and maximum h/R_c is are 0.91 and 1.07 for droplet on wall with temperature slope of -8 k/mm. However, these are 0.92 and 1.06 for droplet on wall with temperature slope of 8 k/mm.

(2). During the evaporation process, there is a turning point, before which the ratio between the droplet height and the radius of the three-phase contact line (h/R_c), the average velocity and the average surface temperature are higher when the wall temperature slope is positive. After the turning point, these are reversed. For h/R_c and the velocity in the droplet, the turning points are t*=1.63×10^{-4} and t*=1.05×10^{-4} for the average surface temperature, respectively.

(3). There are two high-velocity regions in the evaporating droplet, which are at the droplet axis and near the surface. And there are two turning points for velocity in droplet, which are t*=1.63×10^{-4} and t*=1.7×10^{-5} for both maximum velocity and average velocity.

(4). The droplet morphology changes more obviously when the temperature coefficient of the surface tension is greater. In addition, the turning point is delayed from t*=6.41×10^{-5} while α is 8 K/mm to t*=7.91×10^{-5} while α is -8 K/mm, which indicates that the negative wall temperature slope is beneficial for inhibiting the Marangoni effect. The viscous resistance is more obvious inside the droplet with higher viscosity.

It is worth indicating that the focus of the current study is the influence mechanism of the wall temperature distribution on the droplet evaporation process, not the application. In practice, droplet evaporation has an important impact on related applications. Thus, it is worth paying attention to droplet evaporation on walls with different temperature distributions in the context of practical applications. In addition to the constant contact angle model is adopted in the current study, the constant contact line model is another important model. In future research, this model will be considered.

CONFLICT OF INTEREST

The authors declare that they have no conflicts of interest.

AUTHORS CONTRIBUTION

Z. G. Lei: Conceptualization, Investigation, Writing original draft. **C. Q. Shen**: Investigation, Methodology, Writing original draft. **C. C. Song**: Methodology, Software, Validation, Investigation. **F. Yao**: Validation, Investigation. **X. D. Liu**: Writing review & editing, Supervision, Project administration.

REFERENCES

Albernaz, D. L., Amberg, G., & Do-Quang, M. (2016). Simulation of a suspended droplet under evaporation with Marangoni effects. *International Journal of Heat and Mass Transfer*, *97*, 853-860. https://doi.org/10.1016/j.ijheatmasstransfer.2016.02.073.

Al-Sharafi A., Sahin, A. Z., Yilbas, B. S., & Shuja, S. Z. (2016a). Marangoni convection flow and heat

transfer characteristics of water-CNT nanofluid droplets. *Numerical Heat Transfer, Part A: Applications*, *69*, 763-780. https://doi.org/10.1080/10407782.2015.1090809.

Al-Sharafi, A., Yilbas, B. S., Ali, H., & Sahin, A. Z. (2016b). Internal fluidity of a sessile droplet with the presence of particles on a hydrophobic surface. *Numerical Heat Transfer, Part A: Applications*, *70*, 1118-1140. https://doi.org/10.1018/10407782.2016.1230416.

Barmi, M. R., & Meinhart, C. D. (2014). Convective flows in evaporating sessile droplets. *Journal of Physical Chemistry B*, *118*, 2414-2421. https://doi.org/10.1021/jp408241f.

Bi, S. S., Cui, J. W., Ma, L. J., Zhao, G. J., & Wu, J. T. (2016). Thermophysical properties of HFE7100 and HFE7500. *Ciesc Journal*, 67, 1680-1686. https://doi.org/10.11949/j.issn.0438-1157.20151505.

Bi, W., Wu, X., & Yeow, E. K. (2012). Unconventional multiple ring structure formation from evaporation-induced self-assembly of polymers. *Langmuir*, 28, 11056-11063. https://doi.org/10.1021/la300697w

Chandramohan, A., Dash, S., Weibel, J. A., Chen, X., & Garimella, S. V. (2016). Marangoni convection in evaporating organic liquid droplets on a nonwetting substrate. *Langmuir*, 32, 4729-4735. https://doi.org/10.1021/acs.langmuir.6b00307.

Chang, S. T., & Velev, O. D. (2006). Evaporation-induced particle microseparations inside droplets floating on a chip. *Langmuir*, *22*, 1459-1468. https://doi.org/10.1021/la052695t.

Cheng, P., & Wu, H. Y. (2006). Mesoscale and microscale phase-change heat transfer. *Advances in heat transfer*, *39*, 461-563. https://doi.org/10.1016/S0065-2717(06)39005-3

Dai, B. M., Qi, H. F., Liu, S. C., Zhong, Z. F., Li, H. L., Song, M. J., Ma, M. Y., & Sun, Z. L. (2019). Environmental and economical analyses of transcritical CO2 heat pump combined with direct dedicated mechanical subcooling (DMS) for space heating in China. *Energy Conversion and Management*, *198*, 111317. https://doi.org/10.1016/j.enconman.2019.01.119

Dai, B. M., Wang, Q., Liu, S. C., Wang, D. B., Yu, L. Q., Li, X. H., & Wang, Y. Y. (2023). Novel configuration of dual-temperature condensation and dual-temperature evaporation high-temperature heat pump system: Carbon footprint, energy consumption, and financial assessment. *Energy Conversion and Management*, *292*, 117360. https://doi.org/10.1016/j.enconman.2023.117360

Deegan, R. D., Bakajin, O., Dupont, T., Huber, G., Nagel, S., & Witten, T. (1997). Capillary flow as the cause of ring stains from dried liquid drops. *Nature*, *389*, 827-829. https://doi.org/10.1038/39827.

Deegan, R. D., Bakajin, O., Dupont, T., Huber, G., Nagel, S., & Witten, T. (2000). Contact line deposits in an evaporating drop. *Physical Review E*, *62*, 756-765. https://doi.org/10.1103/PhysRevE.62.756.

Deegan, R. D. (2000). Pattern formation in drying drops. *Physical Review E*, *61*, 475-485. https://doi.org/10.1103/PhysRevE.61.475.

Erbil, H. Y., Mchale, G., & Newton, M. I. (2002). Drop evaporation on solid surfaces: constant contact angle mode. *Langmuir*, *18*, 2636-2641. https://doi.org/10.1021/la011470p.

Gao, M., Kong, P., & Zhang, L. X. (2018). Evaporation dynamics of different sizes sessile droplets on hydrophilic and hydrophobic heating surface under constant wall heat fluxes conditions. *International Communications in Heat and Mass Transfer*, *93*, 93-99. https://doi.org/10.1016/j.icheatmasstransfer.2018.03.007

Girard, F., Antoni, M., Faure, S., & Steinchen, A. (2006). Evaporation and Marangoni driven convection in small heated water droplets. *Langmuir*, *22*, 11085-11091. https://doi.org/10.1021/la061572l.

Girard, F., Antoni, M., & Sefiane, K. (2008). On the effect of Marangoni flow on evaporation rates of heated water drops. *Langmuir*, *24*, 9207-9210. https://doi.org/10.1021/la801294x

Guéna, G., Allançon, P., & Cazabat, A. M. (2007). Receding contact angle in the situation of complete wetting: Experimental check of a model used for evaporating droplets. *Colloids and Surfaces A: Physicochemical and Engineering Aspects*, *300*, 307-314. https://doi.org/10.1016/j.colsurfa.2007.02.009.

Hu, H., & Larson, R. G. (2005). Analysis of the effects of Marangoni stresses on the microflow in an evaporating sessile droplet. *Langmuir*, *21*, 3972-3980. https://doi.org/10.1021/la0475270.

Hu, H., & Larson, R. G. (2002). Evaporation of a sessile droplet on a substrate. *The Journal of physiacal chemistry*, *106*, 1334-1344. https://doi.org/10.1021/jp0118322.

Hu, H., & Larson, R. G. (2006). Marangoni effect reverses coffee-ring depositions. *Journal of Physical Chemistry B*, *110*, 7090-7094. https://doi.org/10.1021/jp0609232.

Hu, W. R., & Imaishi N. (2000). Thermocapillary flow in an annular liquid layer painted on a moving fiber. *International Journal of Heat and Mass Transfer*, *43*, 4457-4466. https://doi.org/10.1016/S0017-9310(00)00026-0.

Huang, Y., Zhang, C., & Meng, S. (2022). Molecular origin of fast evaporation at the solid–water–vapor line in a sessile droplet. *Nanoscale*, *14*, 2729-2734. https://doi.org/10.1039/D1NR07479B

Kus, A., Isik, Y., Cakir, M. C., Coşkun, S., & Özdemir, K. (2015). Thermocouple and infrared sensor-based measurement of temperature distribution in metal cutting. *Sensors*, *15*, 1274-1291. https://doi.org/10.3390/s150101274.

Kita, Y., Askounis, A., Kohno, M., Takata, Y., Kim, J., & Sefiane, K. (2016). Induction of Marangoni convection in pure water drops. *Applied. Physics Letters*, *109*, 171602. https://doi.org/10.1063/1.4966542.

Liu, B., Li, Z., Bi, L., Theodorakis, P. E., Liu, Y., Song, J., Chen, A., Zhu Z., & Song, J. (2023). Characteristics of HFE7100 droplets evaporation on substrates with different thermal conductivity. *Thermal Science and Engineering Progress*, *40*, 101771. https://doi.org/10.1016/j.tsep.2023.101771

Machrafi, H., Lyulin, Y., Iorio, C. S., Kabov, O., & Dauby, P. C. (2018). Numerical parametric study of the evaporation rate of a liquid under a shear gas flow: Experimental validation and the importance of confinement on the convection cells and the evaporation rate. *International Journal of Heat and Fluid Flow*, *702*, 8-19. https://doi.org/10.1016/j.ijheatfluidflow.2018.05.003.

Manetti, L. L., Ribatski, G., de Souza, R. R., & Cardoso, E. M. (2020). Pool boiling heat transfer of HFE-7100 on metal foams. *Experimental Thermal and Fluid Science*, *113*, 110025. https://doi.org/10.1016/j.expthermflusci.2019.110025

McHale, G., Rowan, S. M., Newton, M. I., & Banerjee, M. K. (1998). Evaporation and the wetting of a low-energy solid surface. *The Journal of Physical Chemistry B*, *102*, 1964-1967. https://doi.org/10.1021/jp972552i.

Nerger, B. A., Brun, P. T., & Nelson, C. M. (2020). Marangoni flows drive the alignment of fibrillar cell-laden hydrogels. *Science advances*, *6*, eaaz7748. https://doi.org/10.1126/sciadv.aaz7748

Quo, K. H., Uemura, T., & Yang, W. J. (1985). Reflection-interference method to determine droplet profiles. *Applied Optics*, *24*, 2655-2659. https://doi.org/10.1364/ao.24.002655.

Ristenpart, W. D., Kim, P. G., Domingues, C., Wan, J., & Stone, H. A. (2007). Influence of substrate conductivity on circulation reversal in evaporating drops. *Physical Review letters*, *99*, 234502. https://doi.org/10.1103/PhysRevLett.99.234502.

Savino, R., & Fico, S. (2004). Transient Marangoni convection in hanging evaporating drops. *Physics of Fluids*, *16*, 3738-3754. https://doi.org/10.1063/1.1772380.

Savino, R., Paterna, D., & Favaloro, N. (2002). Buoyancy and Marangoni effects in an evaporating drop. *Journal of Thermophysics and Heat Transfer*, *16*, 562-574. https://doi.org/10.2514/2.6716.

Scardovelli, R., & Zaleski, S. (1999). Direct numerical simulation of free-surface and interfacial flow. *Annual Review of Fluid Mechanics*, *31*, 567-603. https://doi.org/10.1146/annurev.fluid.31.1.567

Scriven, L. E., & Sternling, C. V. (1960). The marangoni effects. *Nature*, *187*, 186-188. https://doi.org/10.1038/187186a0.

Sefiane, K., Moffat, J. R., Matar, O. K., & Craster, R. V. (2008). Self-excited hydrothermal waves in evaporating sessile drops. *Applied Physics Letters*, *93*, 074103. https://doi.org/10.1063/1.2969072

Shi, W., Tang, K., Ma, J., Jia, Y., Li, H., & Feng, L. (2017). Marangoni convection instability in a sessile droplet with low volatility on heated substrate. *International Journal of Thermal Sciences*, *117*, 274-286. https://doi.org/10.1016/j.ijthermalsci.2017.04.007.

Shi, X., Lin, L., Chen, S., Chao, S., Zhang, W., & Meldrum, D. (2011). Real-time PCR of single bacterial cells on an array of adhering droplets. *Lab on a Chip*, *11*, 2276-2281. https://doi.org/10.1039/c1lc20207c.

Song, H., Lee, Y., Jin, S., S., Kim, H. Y., & Yoo, J. Y. (2011). Prediction of sessile drop evaporation considering surface wettability. *Microelectronic Engineering*, 88, 3249-3255. https://doi.org/10.1016/j.cis.2013.08.006

Strizhak, P. A., Volkov, R. S., Misyura, S. Y., Lezhnin, S. I., & Morozov, V. S. (2018). The role of convection in gas and liquid phases at droplet evaporation. *International Journal of Thermal Sciences*, *134*, 421-439. https://doi.org/10.1016/j.ijthermalsci.2018.08.031.

Tekin, E., de Gans, B. J., & Schubert, U. S. (2004). Ink jet printing of polymers from single dots to thin film libraries. *Journal of Materials chemistry*, *14*, 2627-2632. https://doi.org/10.1039/b407478e.

Thiele, U., & Knobloch, E. (2004) Thin liquid films on a slightly inclined heated plate. *Physica D: Nonlinear Phenomena*, *190*, 213-248. https://doi.org/10.1016/j.physd.2003.09.048.

Tsoumpas, Y., Dehaeck, S., Rednikov, A., & Colinet, P. (2015). Effect of marangoni flows on the shape of thin sessile droplets evaporating into air. *Langmuir*, *31*, 13334-13340. https://doi.org/10.1021/acs.langmuir.5b02673.

Wang, H. T., Wang, Z. B., Huang, L. M., Mitra, A., & Yan, Y. S. (2001). Surface patterned porous films by convection-assisted dynamic self-assembly of zeolite nanoparticles. *Langmuir*, *17*, 2572-2574. https://doi.org/10.1021/la0102509.

Wang, T. S., & Shi, W. Y. (2020). Transition of Marangoni convection instability patterns during evaporation of sessile droplet at constant contact line mode. *International Journal of Heat and Mass Transfer*, *148*, 119138.

https://doi.org/10.1016/j.ijheatmasstransfer.2019.119138.

Xu, X., Di, Y., & Yu, H. (2018). Sharp-interface limits of a phase-field model with a generalized Navier slip boundary condition for moving contact lines. *Journal of Fluid Mechanics*, *849*, 805-833. https://doi.org/10.1017/jfm.2018.428

Xu, X. F., Luo, J. B., & Guo, D. (2012). Radial-velocity profile along the surface of evaporating liquid droplets. *Soft Matter*, *8*, 5797-5803. https://doi.org/10.1039/c2sm25319d.

Xu, Y., Zhang, N., Yang, W. J., & Vest, C. M. (1984). Optical measurement of profile and contact angle of liquids on transparent substrates. *Experiments in Fluids*, *2*, 142-144. https://doi.org/10.1007/bf00296430.

Yang, K., Hong, F. J., & Cheng, P. (2014). A fully coupled numerical simulation of sessile droplet evaporation using Arbitrary Lagrangian–Eulerian formulation. *International Journal of Heat and Mass Transfer*, *70*, 409-420. https://doi.org/10.1016/j.ijheatmasstransfer.2013.11.017.

Yin, J., Ye, H., Xia, X., Yi, L., & Wang, T. (2023). Methanol–water mixture evaporation-induced self-assembly of ZIF-8 particles. *Chemical Communications*, *59*, 11508-11511. https://doi.org/10.1039/D3CC03357K

Zhang, J., Huang, H., & Lu, X. Y. (2019). Pinning–depinning mechanism of the contact line during evaporation of nanodroplets on heated heterogeneous surfaces: A molecular dynamics simulation. *Langmuir*, *35*, 6356-6366. https://doi.org/10.1021/acs.langmuir.9b00796

Zhang, M., Liu, Z. L., Ma, G. Y., & Cheng, S. Y. (2009). Numerical simulation and experimental verification of a flat two-phase thermosiphon. *Energy Conversion and Management*, *50*, 1095-1100. https://doi.org/10.1016/j.enconman.2008.12.001.

Zhang, Z., Li, J., & Jiang, P. X. (2013). Experimental investigation of spray cooling on flat and enhanced surfaces. *Applied Thermal Engineering*, *51*, 102-111. https://doi.org/10.1016/j.applthermaleng.2012.08.057.

Zhu, J. L., Shi, W. Y., & Feng, L. (2019). Bénard-Marangoni instability in sessile droplet evaporating at constant contact angle mode on heated substrate. *International Journal of Heat and Mass Transfer*, *134*, 784-795. https://doi.org/10.1016/j.ijheatmasstransfer.2019.01.082.

Zhu, J. L., & Shi, W. Y. (2023). Instability patterns of Marangoni flow in evaporating droplets on lyophobic surface. *International Communications in Heat and Mass Transfer*, *141*, 106598. https://doi.org/10.1016/j.icheatmasstransfer.2022.106598